Phil. Trans. R. Soc. Lond. B **289**, 489–500 (1980) [489]
Printed in Great Britain

Field focusing n.m.r. (FONAR) and the formation of chemical images in man

BY R. DAMADIAN
Department of Medicine and Program in Biophysics, State University of New York, Downstate Medical Center, 450, Clarkson Avenue, Brooklyn, New York 11203, *U.S.A.*

[Plates 1–3]

The first proposals for n.m.r. scanning in medical diagnosis were made by Damadian (1971*a*; 1972) and were followed by Lauterbur (1973). Damadian's method of scanning used the principle that the forced precessions of a nuclear magnetization under radio frequency (r.f.) driving field specify the conditions for obtaining spatial resolution of the signal producing domains of a nuclear resonance sample. Sufficient coupling of the nuclear spins to the radiation field to produce a signal detectable by r.f. spectroscopy requires that the stringent Bohr frequency condition, $h\nu = \mu H_0/I$, be met. It became possible to construct, with the aid of direct current auxiliary coils, a small volume, called the resonance aperture, inside the applied static field of the magnetic resonance experiment. The correct value of H_0 for the applied frequency is restricted to this aperture. The technique (Damadian 1972) was developed to provide a method for non-surgically detecting chemical abnormalities in the diseased organs of patients (Damadian 1971*a*). The first n.m.r. scans of normal patients and of those with malignant disease are discussed.

N.m.r. scanning for medical diagnosis was first proposed in 1971 (Damadian 1971*a*). The rapid development of this idea from its first conception by Damadian in 1969 to its final practical realization in the body scanning machines making their appearance in our laboratory (Damadian *et al.* 1977, 1978) and others around the world (Mansfield *et al.* 1978; Mallard *et al.* 1979) reflects its medical promise. In a larger sense, the development represents a major transformation of medical philosophy, the full impact of which on medicine and society will not be evident for a half century or more.

The opportunity to test the idea came in the summer of 1970. The first experiments were aimed at answering the question 'Can the n.m.r. signal detect disease?' and were performed by me on the premises of N.M.R. Specialties in New Kensington, Pennsylvania.

Two groups of rats with malignant tumours were studied, one infected with Walker sarcoma and the other with Novikoff hepatoma. The tumours were surgically removed and put in n.m.r. tubes. Spin–lattice and spin–spin constants of hydrogen for the tumours and for a range of normal rat tissues were measured. The T_1 results are shown in table 1.

Two malignancies, a Novikoff hepatoma and a Walker sarcoma, had T_1 values that fell entirely outside the range of normal tissues. No instances of overlap were encountered. This set of experiments established that the n.m.r. signal could detect disease and the n.m.r. body scanning idea came to life (Damadian 1971).

Apparatus to achieve the body scanning objective had to satisfy a new condition not required in the measurements on excised tissues and not provided by 'state of the art' n.m.r. instruments. An n.m.r. method was required for 'in-sample' focusing that could spatially locate the tumour within the body and provide a means for directing the n.m.r. beam to specific sites within the anatomy for a locus by locus examination of tissue chemistry.

The focusing n.m.r. (or FONAR) concept arises from the implicit constraints on the forced precessions of a nuclear magnetization in an r.f. driving field. These constraints provide the basis for obtaining spatial resolution of the signal producing domains of a nuclear resonance sample. Sufficient coupling of the nuclear spins to the radiation field to produce a signal detectable by r.f. spectroscopy requires that the stringent Bohr frequency condition, $h\nu = \mu H_0/I$, be met. It is thus possible to develop a small volume in the working field of the static magnet that contains the correct values of H_0 to bracket the band of the r.f. pulse.

TABLE 1. RODENT T_1 (HYDROGEN) RELAXATIONS

(Reproduced from Damadian (1971).)

	muscle	liver	stomach	small intestine	kidney	brain
normal	0.538 ± 0.015	0.293 ± 0.010	0.270 ± 0.016	0.257 ± 0.030	0.480 ± 0.026	0.595 ± 0.007
tumour	0.736 ± 0.002	0.826 ± 0.013				
	Walker sarcoma	Novikoff hepatoma				

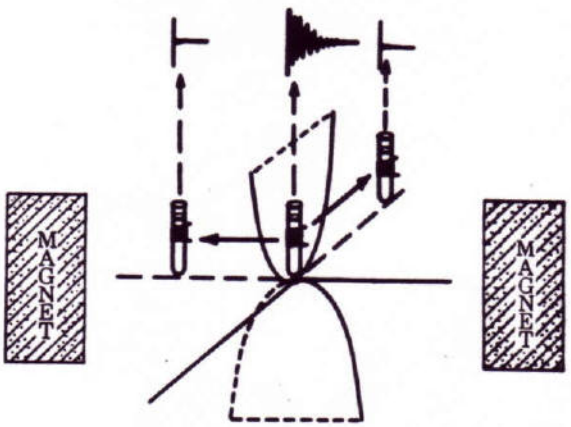

FIGURE 1. Principle of the FONAR method is illustrated. Centring the n.m.r. sample in the magnet produces good signal (shown above the centred sample). Moving the sample too far off centre causes it to vanish.

The principle of the FONAR method is illustrated in figure 1 and exploits the same property of standard n.m.r. machines that trips beginners learning to use the apparatus for the first time. Novices discover early that failure to carefully place the n.m.r. probe and sample at the centre of the magnetic field produces poor signal or none at all. Centring it produces good signal (shown above the centred sample in figure 1). Moving the sample too far off-centre causes the signal to vanish. Application of this principle to human body scanning requires that the sample (body) be moved with respect to the magnet so as to move the signal-generating volume of the magnet through different regions and organs of the body, as first stated in Damadian (1971) Figure 7 shows the final form of the apparatus for body scanning by this means.

A field plot of our present FONAR magnet and coils illustrates the FONAR concept more deliberately. A plot of field intensity in the mapping plane of the FONAR n.m.r. scan shows the field to be approximately saddle-shaped. In this figure vertical height is field intensity while the z axis is horizontal and x is into the plane of the paper. When the n.m.r. pick-up coil is tuned for resonance at the field value of the saddle point, all parts of the sample lying outside the

saddle point will either be immersed in a field of different intensity and not give resonance or be in a region of the field that is too steeply graded to generate signal. The locus of all points in the field mesh isomagnetic with the saddle point are drawn as dotted lines. These are obtained by cutting across the surface with a plane parallel to the base and passing through the saddle point. The plane is the locus of all points at the same altitude as the saddle point and therefore represents the plane containing all points of magnetic intensity equal to the saddle point. The locus of all points on the saddle surface that are isomagnetic with the centre point is the intersection of this plane with the surface and represents all the off-centre elements that could satisfy resonance. It can be seen by examining the figure that the off-centre elements fall on curvatures of the field that are too steeply graded to give resonance.

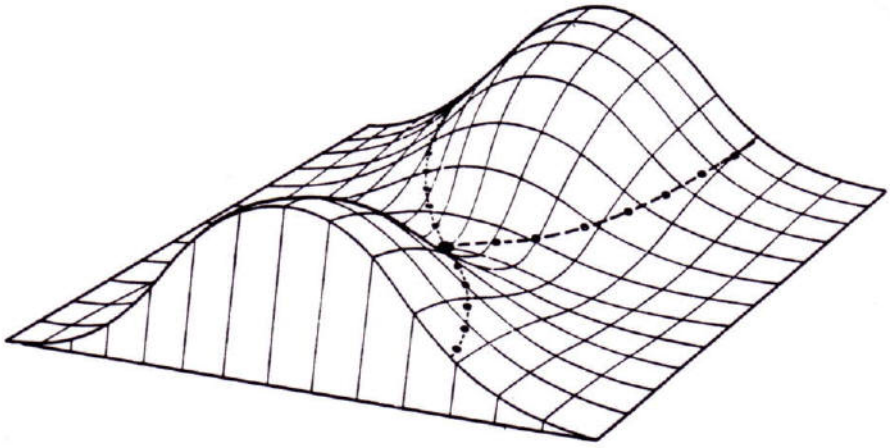

FIGURE 2. A field plot of the FONAR magnet and coils.

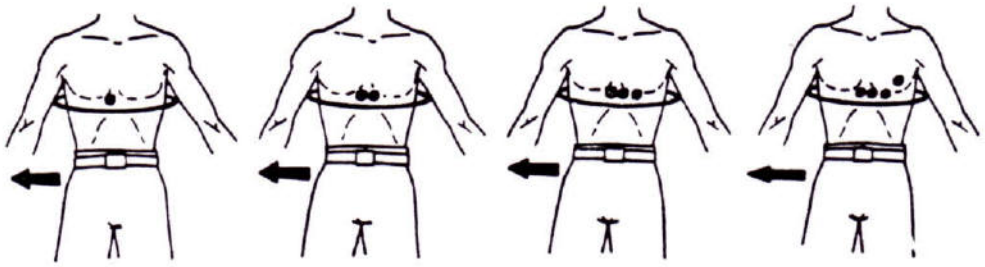

FIGURE 3. In this illustration the torso of the human sample is first centred on the resonance aperture. Data is recorded on the n.m.r. signal at the start location, the coordinates stored and the sample translated to the next location. The data collection process is then repeated with the resonance aperture at the new location. At the end of a scanning line, the resonance aperture is positioned at the start of a new line by a right-angle translation. The process is repeated until a rectangular grid of scanning elements has been completely traversed.

A pair of these contour lines, orthogonal to each other and passing through the origin, where the saddle point is located, illustrates the principle in figure 1.

As shown in figure 1, when the exploring n.m.r. sample is at the plateau of the conic section a signal is produced both because the resonant frequency is tuned to H_0 and because there is sufficient H_0 uniformity to produce it. The signal vanishes when moved off-centre along either axis because H_0 departs from the field value of resonance and because the field is too steeply graded to generate signal.

The principle shown in figure 3 illustrates the process as it operates during a FONAR body scan. In this illustration the torso of the human sample is first centred on the resonance aperture. Data is recorded on the n.m.r. signal at the start location, the coordinates stored and the sample translated to the next location. The data collection process is then repeated with the resonance aperture at the new location. At the end of a scanning line, the resonance aperture is positioned at the start of a new line by a right angle translation. The process is repeated until a rectangular grid of scanning elements has been completely traversed.

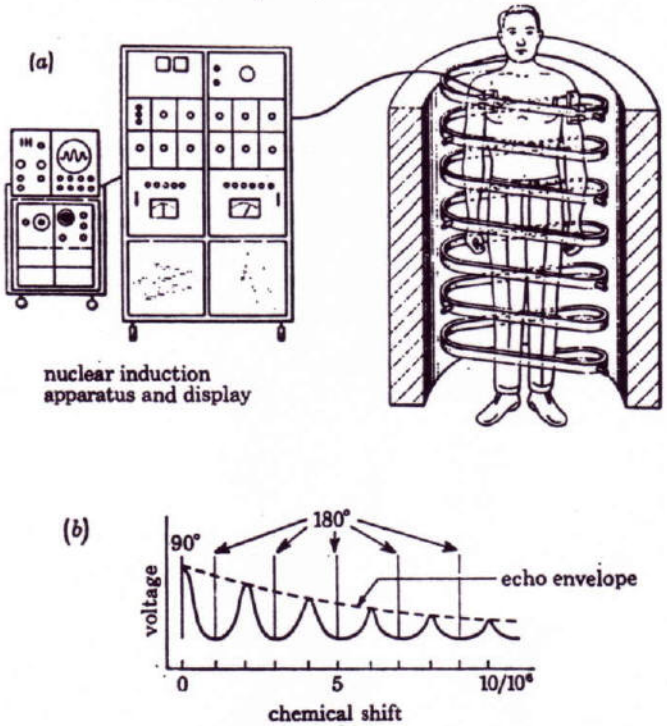

FIGURE 4. Face sheet on the U.S. patent 3,789,832 of human n.m.r. scanning.

TABLE 2. RODENT ^{23}Na N.M.R. (SIGNAL INTENSITY)

(Reproduced from Goldsmith & Damadian (1975).)

	muscle	liver	intestine	lung	kidney	testis
normal	76±7	90±7	124±11	134±12	189±9	155±10
tumour	219±34	257±24	213±9	363±18		
	Walker sarcoma	Novikoff hepatoma	sarcoma 180	Ehrlich ascites		

A description of the invention of human n.m.r. scanning was filed for United States patent in 1972 (Damadian 1972) (see figure 4).

Further explorations in tissue for elements other than hydrogen that would be useful nuclear probes of disease demonstrated the utility of the sodium nucleus. The amplitude of the tumour sodium signal substantially exceeded the amplitude of the normal signal (see table 2).

For phosphorus, the result was similar to that for water. The T_1 relaxations were greater in tumours than in normal tissues (see table 3).

Beyond pulsed measurements of relaxation times, n.m.r. spectral methods were applied to obtaining tissue chemistry and proved informative.

Hoult's classical 1974 paper (Hoult *et al.* 1974), which worked out the ^{31}P spectrum of normal muscle and identified the molecular origin of the spectral lines in the muscle spectrum, provided us with the opportunity to compare the ^{31}P spectrum of malignant muscle with that of the normal tissue. The ^{31}P spectra obtained by Koutcher from normal and from malignant muscle showed differences (Koutcher & Damadian 1977). The tumour lacked the ATP (see figure 5) and phosphocreatine resonances, while the inorganic and sugar phosphate peaks, A and B, were shifted upfield by 70 and 40 Hz respectively.

TABLE 3. RODENT T_1 (PHOSPHORUS) RELAXATIONS

(Reproduced from Zaner & Damadian (1975).)

	liver	muscle	brain	kidney	intestine
normal	2.33 ± 0.14	2.19 ± 0.05	1.13 ± 0.05	1.43 ± 0.15	1.97 ± 0.12
tumour	5.98 ± 0.57	5.38 ± 0.68	5.19 ± 1.42		
	Novikoff hepatoma	Walker sarcoma	sarcoma 180		

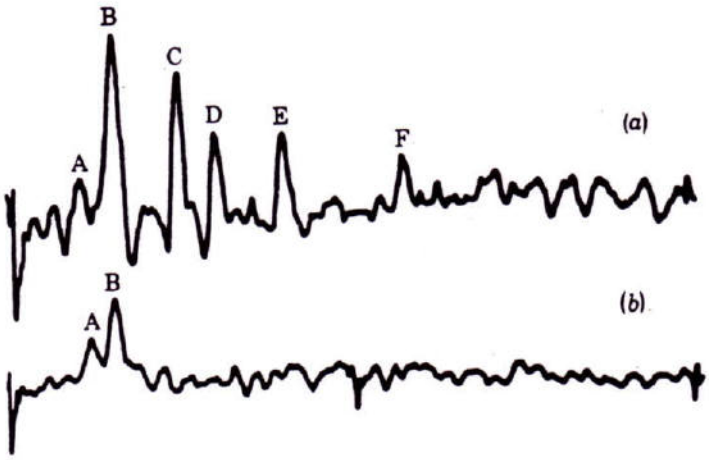

FIGURE 5. (*a*) ^{31}P spectrum of normal skeletal muscle. Sweep width, 5000 Hz; pulse interval, 10 s; 256 averaged f.i.ds (free induction decays). Peak positions based on the mean position of eight separate experiments. A: sugar phosphate; chemical shift, -3.9×10^{-6}. B: P_i; -1.7×10^{-6}. C: creatine phosphate; 3.1×10^{-6}. D: γ phosphate of ATP; 5.6×10^{-6}. E: α phosphate of ATP; 10.8×10^{-6}. F: β phosphate of ATP; 19.6×10^{-6}. (*b*) ^{31}P spectrum of cancer of muscle (mouse rhabdomyosarcoma). Sweep width, 5000 Hz; pulse interval, 5 s; 512 averaged f.i.ds. Peak assignments and positions based on the mean position of five separate experiments. A: sugar phosphates; chemical shifts, -4.3×10^{-6}. B: P_i: -2.4×10^{-6}.

In a large investigation of human tissues, T_1, T_2 and $T_{1\rho}$ were measured in 1000 biopsy specimens taken at surgery. The same general results were obtained in these relaxation determinations of human tissue as in rodent tissue, but with more variation. The increased variance is presumably due to the marked variance in the clinical state of patients with cancer as compared with laboratory animal populations. The latter are as near to homogeneous experimental populations as possible. In a typical laboratory animal study, experimental rodents are litter mates of the same age and strain, share the same food and water, are inoculated with cancer on the same day and are commonly tested for disease on the same day after inoculation. The data from the human T_1 measurements are shown in tables 4, 5 and 6.

In 1973, Lauterbur's method for n.m.r. scanning (Lauterbur 1973) was published and was quickly followed by Mansfield's invention of n.m.r. diffraction (Mansfield & Grannel 1973) and Hinshaw's invention of sensitive point imaging (Hinshaw 1974).

Lauterbur's picture of the mouse lent support to the idea of human body scanning (Damadian 1971, 1972), but failed to answer the basic objections to human body scanning, which centred around the practicability of body size uniform magnetic fields, tissue penetrability of r.f. and the diminished signal : noise characteristics of large probe coils.

TABLE 4. HUMAN (MUSCLE AND CONNECTIVE TISSUE) T_1 RELAXATIONS/S

(Reproduced from Damadian *et al.* (1974) and Goldsmith *et al.* (1978*a*).)

	breast	skin	muscle
normal	0.365 ± 0.079	0.616 ± 0.019	1.023 ± 0.029
tumour	1.080 ± 0.08	1.047 ± 0.108	1.413 ± 0.032

TABLE 5. HUMAN T_1 RELAXATIONS/S

(Reproduced from Damadian *et al.* (1974) and Goldsmith *et al.* (1977).)

haematopoetic	spleen	lymphatic
normal	0.701 ± 0.045	0.720 ± 0.076
tumour	1.113 ± 0.006	1.004 ± 0.056

	lung		bone
normal	0.788 ± 0.063	normal	0.554 ± 0.027
tumour	1.110 ± 0.057	tumour	1.027 ± 0.152

TABLE 6. HUMAN T_1 RELAXATIONS (DIGESTIVE ORGANS)/S

(Reproduced from Damadian *et al.* (1974) and Goldsmith *et al.* (1978*b*).)

	oesophagus	stomach	intestinal tract	liver
normal	0.804 ± 0.108	0.765 ± 0.075	0.641 ± 0.043	0.570 ± 0.029
tumour	0.104	1.238 ± 0.109	1.222 ± 0.04	0.832 ± 0.012

We began construction of the human scanner with fabrication of the magnet, a two coil niobium–titanium superconductive magnet in a Helmholtz pair arrangement with a 4 ft 5 in† (room temperature) bore.

The magnet was wound on an aluminium former made from rolled channel bar. The windings were laid down by means of a winding machine that we had designed and built for the purpose. The machine was designed to feed wire automatically to the turning former by means of a motor-driven lead screw assembly and a motor-driven wire tension control. The time required to wind each magnet was approximately two weeks.

Each magnet half contains a sweep coil and a z-gradient coil in addition to the main magnet windings. The sweep and z-gradient coils consist of two layers, each of Formvar-coated copper-clad niobium–titanium superconducting wire with a 12 mil diameter core and a total diameter of 0.026 in. There are 76 turns to each layer. The main magnet consists of 5 layers of the

† $1\,\text{mil} = 10^{-3}\,\text{in} = 2.54 \times 10^{-2}\,\text{mm} = 2.54 \times 10^{-5}\,\text{m}$; $1\,\text{in} = 2.54\,\text{cm} = 2.54 \times 10^{-2}\,\text{m}$; $1\,\text{ft} = 0.305\,\text{m}$.

same wire (76 turns per layer) and 47 layers (91 turns per layer) of Formvar-coated copper-clad niobium–titanium wire with a core diameter of 10 mil and a total diameter of 22 mil. Each layer is insulated by two wraps of 0.5 mil Mylar ribbon, and the windings are separated from the walls of the former by spacers 250 mil wide and machined from G-10 plastic. The outer layer of windings is secured in place by 0.5 mil Hastaloid ribbon.

TABLE 7. CHARACTERISTICS OF THE HUMAN MAGNET (EACH HALF)

magnet bore diameter	53 in
inductance	61.8 H
stored energy in the magnetic field (at 4 MHz)	2.97×10^4 J
stability (at 2.18 MHz)	7 parts in 10^7 per hour
magnet mass (without Dewar)	120 lb (54.4 kg)
maximum field (theory)	5000 G
maximum field (so far tested)	1000 G

One of the novel features of the magnet is a plate capable of being removed from the Dewar flask while the magnet remains fixed in place. Access to the plate is provided through a demountable header plate in a gooseneck joining the main magnet Dewar flask to the helium reservoir tank. Superconductive joints, persistent switches etc. are thereby all made accessible for repair without dissembly of the Dewar flask. This plate contains all of the superconducting joints as well as the superconducting switches necessary to place the magnet into a 'persistent' mode of operation. In addition, the plate houses all electrical connections necessary for operation of the main magnet and other coils. Also incorporated, and essential to the operation of a magnet of high inductance, are protective devices against a sudden dumping of stored energy, as well as high resistance but low power consuming (less than 300 mW) superconducting switches.

Although the magnet is theoretically capable of attaining a field of approximately 5000 G† according to our computer calculations of the field mesh, our tests generally have been conducted with the magnet in persistent operation at either 500 or 1000 G. A preliminary estimate by n.m.r. of the drift rate of the magnet indicates that it is better than 7 parts in 10^7 over a period of 1 h. In fact, to date there has been no n.m.r.-detectable drift. Table 7 presents a short compilation of the properties of each magnet comprising the Helmholtz pair. Figure 6 shows a hydrogen off-resonance beat pattern obtained in one operating magnet half at 2.18 MHz with a 1 in diameter single coil probe formed from a pair of cylindrical Helmholtz coils.

The cryogen to house the magnet consisted of three sections: the magnet hoop, storage can and a right angle gooseneck joining the two. The magnet hoop was built to maintain the magnet in an upright position, z axis horizontal. The magnet is bolted into the liquid helium can, a doughnut-shaped stainless steel (type 304) tank that we welded closed with a 300-A Airco TIG Heliwelder and thermally isolated by spacers (G-10 plastic, a glass-impregnated epoxy resin). The heat shield (6061-T6 aluminium) surrounding the helium section is conduction-cooled to 77 °K by means of a second concentric doughnut containing liquid nitrogen. The heat shield was polished to a mirror finish to increase reflectivity and reduce helium loss due to radiation. Radiated heat transfer was further reduced by a wrapping of several layers of superinsulation (aluminized Mylar, Metallized Products Division of King-Seeley Co., Winchester, Massachusetts) over the heat shield and also by a layer of aluminium tape (Emerson & Cuming, Canton, Massachusetts) wrapped on the liquid helium can. The nested doughnut sections,

† 1 G = 10^{-4} T.

consisting of the liquid helium magnet can surrounded by the nitrogen-cooled radiation shields, were encased in an outer vacuum jacket made of 6061-T6 aluminium $\frac{1}{2}$ in thick. We welded all the 6061 aluminium joints in the Dewar flask with the 300-A Heliwelder. Seams and final Dewar flask assembly were checked for leaks with a Veeco model MS17-AM helium leak detector and defective seams or porosities elsewhere in the metal were sealed with the welder.

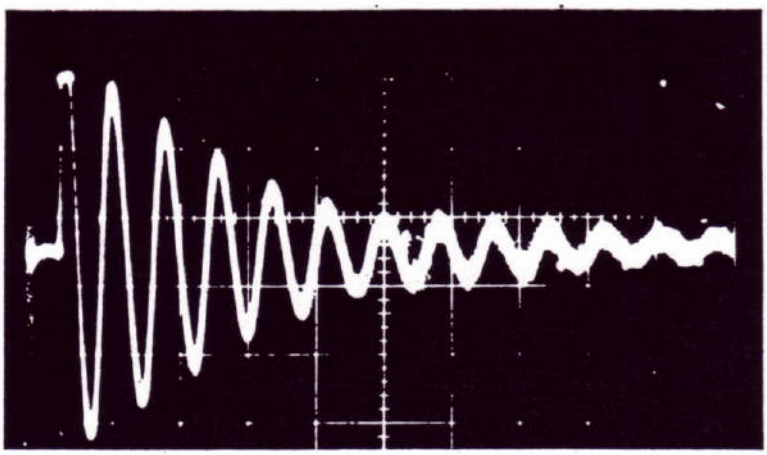

MHz

FIGURE 6. Hydrogen off-resonance beat pattern obtained in one operating magnet half at 2.18 MHz by means of a 1 in diameter single coil probe formed from a pair of cylindrical Helmholtz coils. Vertical scale, 1 V per square. Horizontal scale, 200 μs per square.

The storage can consists of two liquid nitrogen reservoirs, which bracket a liquid helium reservoir. The storage reservoirs for the cryogenic liquids are made of stainless steel (type 304) for strength and low heat conduction. The outer vacuum jacket of the storage can is made of aluminium (6061-T6). Joints between the steel storage cans and the aluminium outer jacket were made using Bi-Braze interfaces obtained from the Bi-Braze Corporation (Glen Head, New York). Pressure manifolds, vents, and fill tubes were necessary to equalize nitrogen levels in the dual tank N_2 storage reservoir and for effective delivery of cryogenic liquid to the hoop. The gooseneck, a 2 in stainless steel tube connecting the helium storage can to the liquid helium reservoir of the hoop, provided an excellent location for placement of the magnet 'persistent' switches and superconductive joints. Repair of joints of persistent switches, when needed, were accomplished through the gooseneck demountable header plate, without dissembly of the main magnet Dewar flask. The addition of flexible metal bellows (Metal Bellows Corp., Sharon, Massachusetts) on the verticle arm of the gooseneck tube permitted easy removal of the switch plate from the helium tube.

The magnet is charged through a pair of 100-A demountable leads (American Magnetic Corp., Oak Ridge, Tennessee) that enter through the helium port in the top of the storage can and mate through a bayonet fitting to the main power leads mounted on a connector panel at the base of the storage can. A demountable Bendix connector, also coupling to the connector panel through the top helium port of the storage can, carries the heater leads for the superconductive switches, the level detector leads for storage can and hoop, and the voltage sensors for monitoring the magnet terminals during charging.

Figure 7, plate 1, shows the completed human scanner.

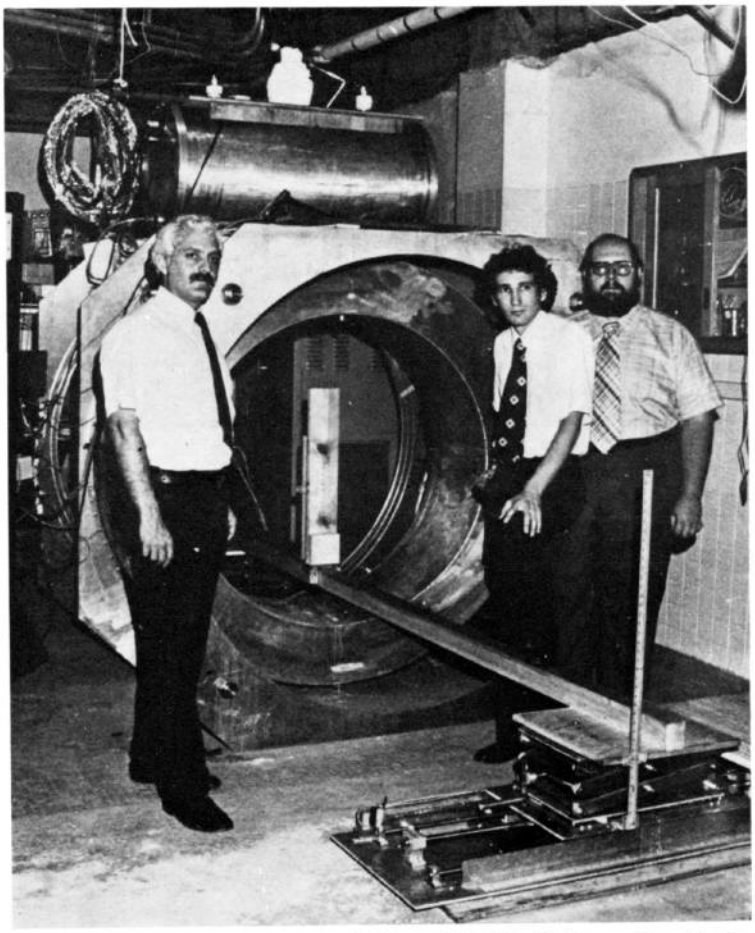

FIGURE 7. Completed human n.m.r. scanner. (Left to right) Dr R. Damadian, Dr. L. Minkoff and Dr M. Goldsmith.

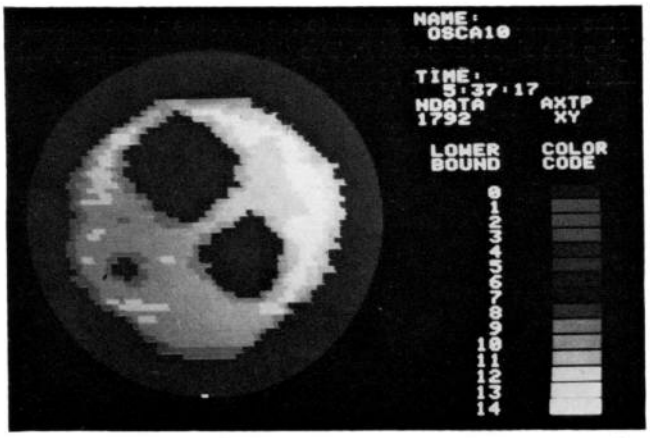

FIGURE 10. Cross-sectional image by focused n.m.r. (FONAR) of simulated chest.

(*Facing p.* 496)

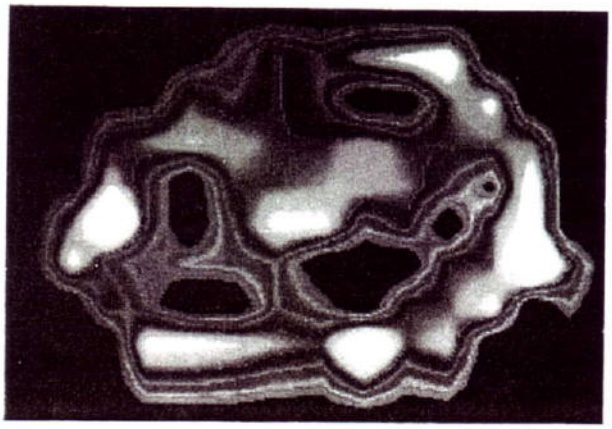

FIGURE 14. FONAR cross-sectional scan through the low chest (10th thoracic vertebra) in a patient with advanced alveolar cell carcinoma. The tumour is seen as intense signal-producing tissue invading both lung cavities and obliterating the bulk of the air space. (Scanning time: 30 min.)

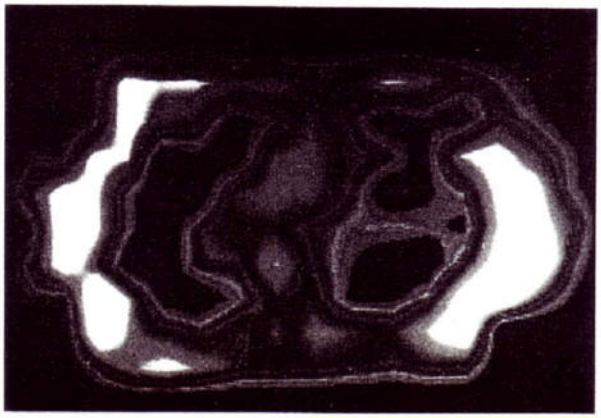

FIGURE 15. FONAR cross-sectional scan through the thorax at the level of the 3rd intercostal space in a patient with an adenocarcinoma of the breast that metastasized to the right lung. The tumour is seen as a band of signal-producing tissue bridging the right lung cavity. The tortuous structure separating the right and left lung cavities is the aortic arch. (Scanning time: 36 min.)

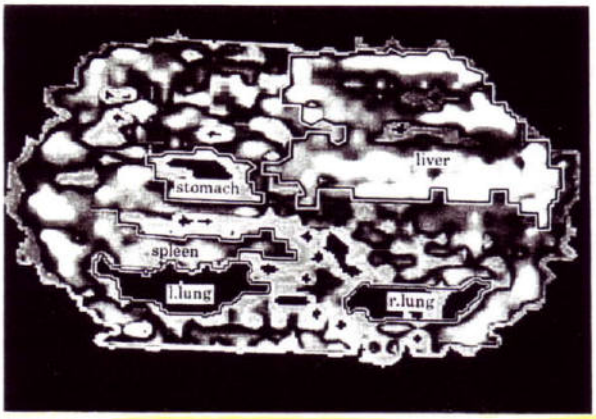

FIGURE 16. FONAR scan of the live human abdomen obtained 11 February 1978. The image, a hydrogen scan obtained at a transmitter frequency of 2.18 MHz, is a section, approximately 4 mm thick, through the abdomen at the level of the 12th thoracic vertebra. The bright shadow in the upper right quadrant of the image corresponds to the liver. The black shadows along the bottom of the figure represent the posterior processes of the right and left lung respectively. The bright peninsular shadow above the left posterior lung field corresponds with the position of the spleen and the smaller black (presumably gas-filled) cavity in the left upper quadrant near the midline is in the vicinity of the stomach.

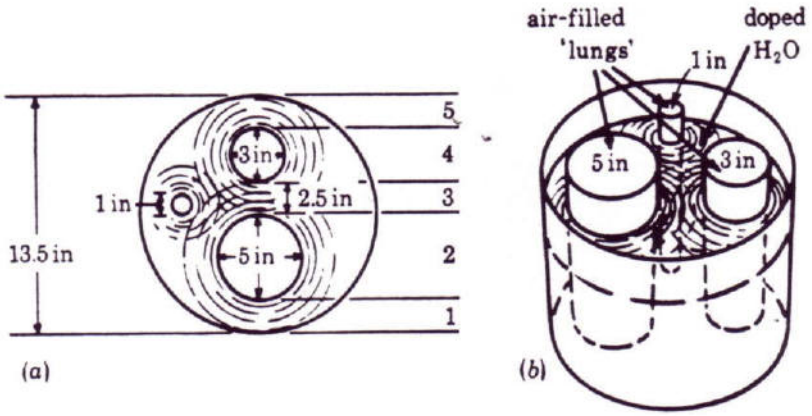

FIGURE 8. Schematic of the simulated (phantom) human chest used to obtain the FONAR image reproduced in figure 10. The phantom consisted of a cylindrical polypropylene tank (13.5 in in diameter) filled with doped H_2O and containing three air-filled lucite cylinders with dimensions as indicated serving as 'lungs'. The numbered regions in the drawing correspond to the position of the FONAR spot for the n.m.r. signals shown in figure 9. Note that the FONAR process easily detected the smallest structure in the phantom (1 in 'lung') with a 14 in exploring coil (see figure 10).

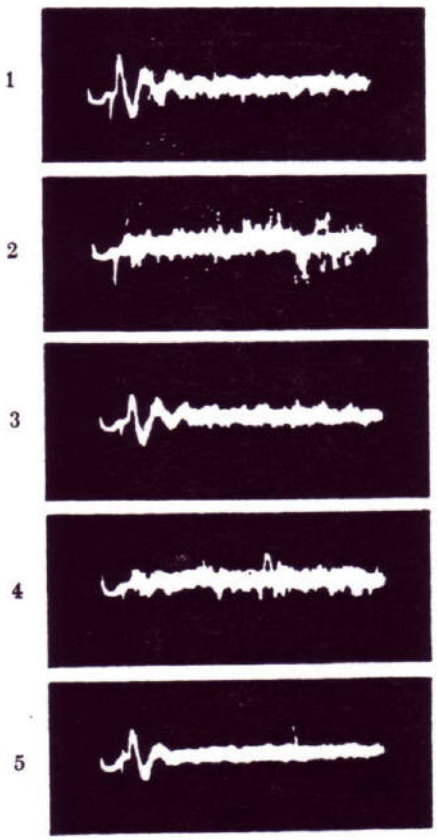

FIGURE 9. Off-resonance proton n.m.r. signals (without signal averaging) from each of the numbered regions of the phantom shown in figure 8.

A trial scan of a phantom chest, figure 8, settled the question of r.f. penetrability of large samples. Visible proton signal (no signal processing) was obtained from all phantom locations.

Figure 9 shows the signal obtained from the numbered regions of the phantom in figure 8. There was no significant attenuation of signal from the interior of the sample (region 3) relative to sample nearest the antenna (regions 1 and 5). Figure 10, plate 1, is the completed FONAR scan of the phantom.

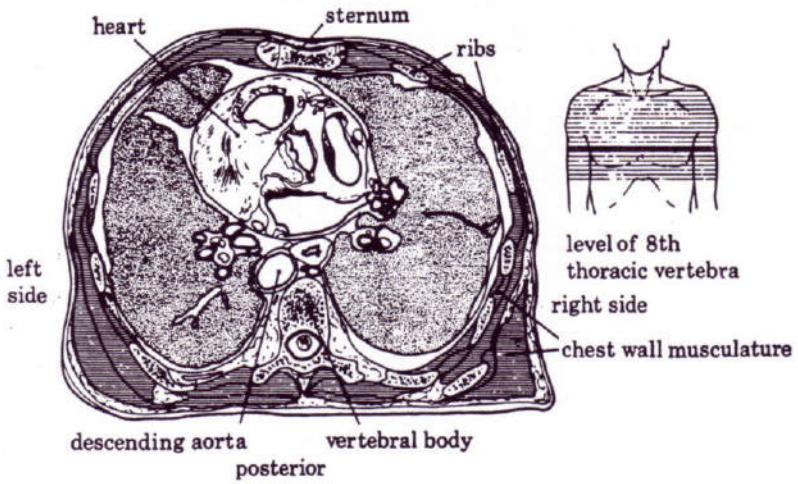

FIGURE 12. Schematic of the human chest at the level of the 8th thoracic vertebra.

I was the subject (on 11 May 1977) for the first attempt at a live human scan. My baseline blood pressure, respiratory rate, pulse rate and electrocardiographic determinations exhibited no significant changes during the scan, which, however, failed because of excessive loading of the antenna by a sample too large for the dimensions of the r.f. coil.

A second attempt at this experiment was successful at 04h 45, 3 July 1977. The scan (see figure 11, plate 3), a cross-section through the chest of Lawrence Minkoff, showed the body wall, the right and left lungs, the heart and its chambers (right atrium and one of its ventricles) and a cut through the descending aorta. Figure 12, a cross-sectional view at the level of the scan, taken from an anatomy text, is shown for comparison.

DESCRIPTION OF PLATE 2

FIGURE 11. A FONAR cross-section of the live human chest at the level of the 8th thoracic vertebra. Proton signal intensity is colour-coded, with dark blue assigned to zero signal amplitude and signals of increasing amplitude taking on the lighter colours toward the yellow and white intensities. Top of image is anterior boundary of chest wall. Left area is left side of chest. Proceeding from anterior to posterior along midline, the principal structure is the heart seen encroaching on the left lung field (blue cavity). Left lung is diminished in size relative to right lung (blue cavity to right of midline), as it should be (see figure 15). More posteriorly and slightly left of midline is a red circular structure corresponding to the descending aorta. In the body wall, beginning at the sternum (anterior midline) and proceeding around the ellipse, alternation of high intensity (yellow) with intermediate intensity (red) could correspond to alternation of intercostal muscles (high intensity) with rib (low intensity) (see figure 12).

FIGURE 13. FONAR scan at the level of 1–¾ in below Angle of Lewis in a man 46 years old with pulmonary oat cell carcinoma. Tumour indicated by light blue infiltrate in left lung field, which should be black as it is in right lung cavity. Midline structure (red) separating the two lung cavities is the cross section through the arch of the aorta.

11

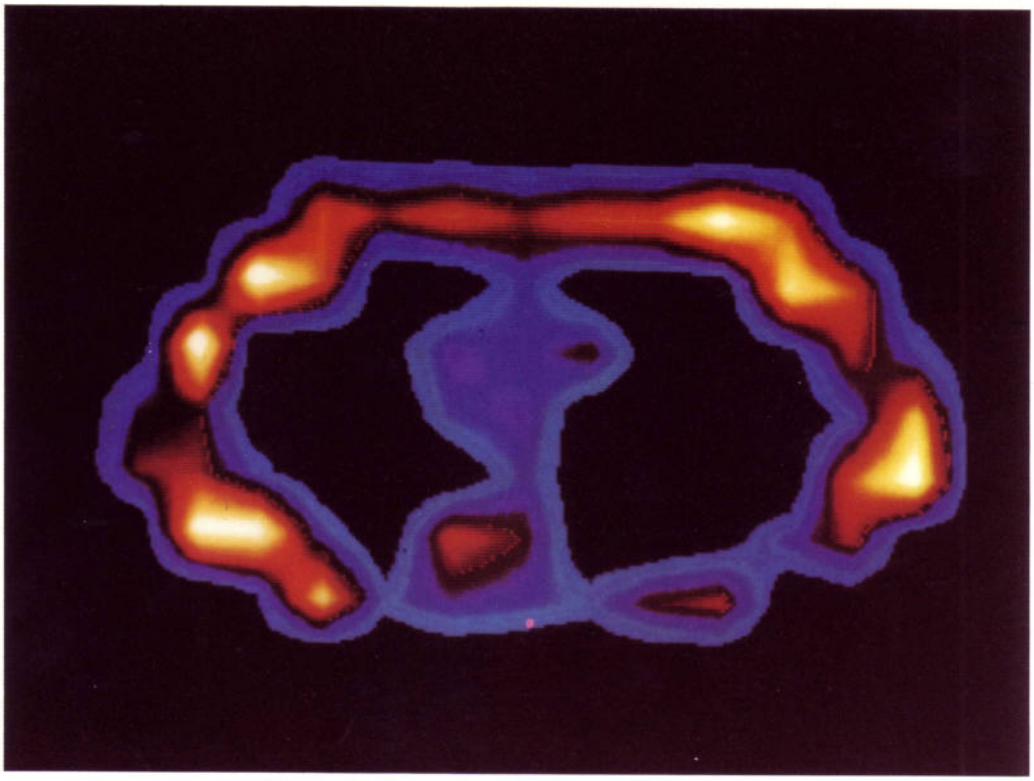

13

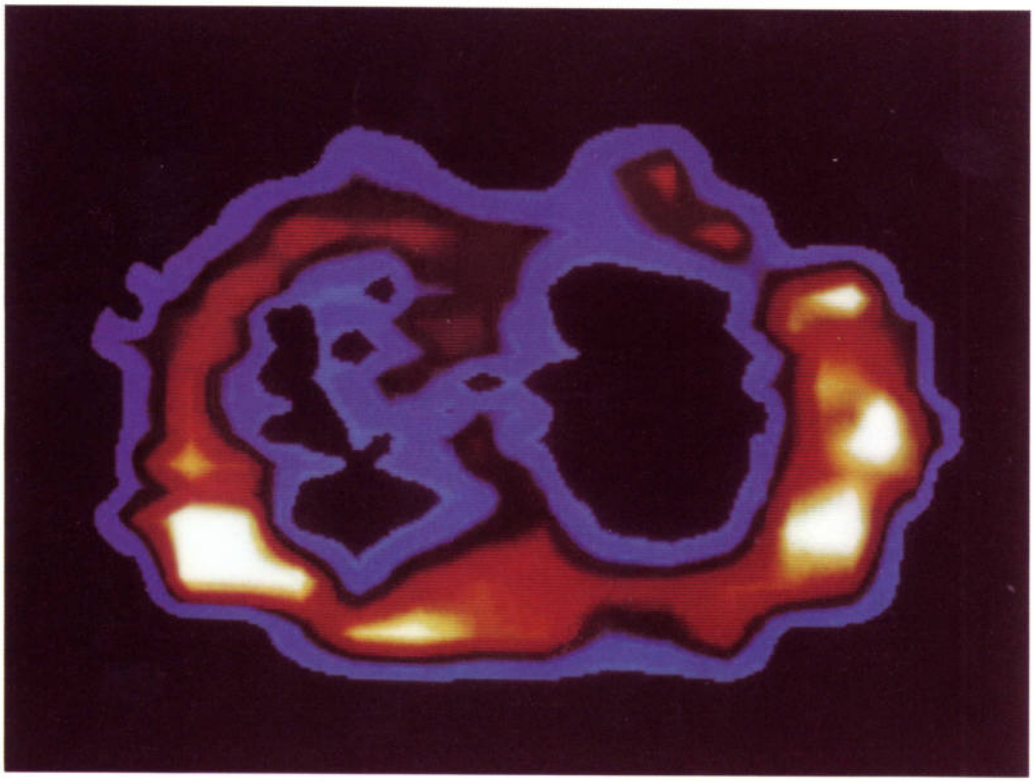

FIGURES 11 AND 13. For description see opposite.

Figure 13, plate 2, contains the scan of a man 46 years old with an oat cell carcinoma invading his left chest. The tumour appears in the scan as signal-producing tissue (blue) infiltrating the left chest.

Figure 14, plate 3, is a cross section through the chest of a patient who was riddled with alveolar cell carcinoma. The tumour is shown as the signal-producing territory invading both lung fields. The patient's chest is assymetric because of a prior thoracotomy on the left side.

Figure 15, plate 3, is a scan through the chest of a 42 year old woman with a small metastasis to the right lung from the breast, shown as a signal-generating lesion bridging the right lung cavity. The section is taken at a level above the heart (and therefore above the breast) and shows the arch of the aorta.

The final image (figure 16, plate 3) is a scan across Lawrence Minkoff's abdomen, an inch below the sternum.

The liver is seen as the large mass in the upper right hand corner. At the bottom of the image are cuts through the posterior portions of the lungs as they ride over the curvature of the diaphragm. On the left is the spleen and anterior to this a gas-filled viscus, which we have identified as the stomach.

Scan time for the first human scan (figure 11) was 4½ h. Subsequent scans were performed in as little as 20 min. Picture resolution is 4–6 mm. The scans were performed at an operating frequency of 2.18 MHz and a magnetic field of 508 G (Damadian *et al.* 1977).

References (Damadian)

Damadian, R. 1971*a* Tumor detection by nuclear magnetic resonance. *Science, N.Y.* **171**, 1151–1153.

Damadian, R. 1971*b* Basic research leads to radio signals from cancer tissue. *Downstate Reporter* **2**, 1.

Damadian, R. 1972 Apparatus and method for detecting cancer in tissue. *U.S. Pat.* no. 3789832, filed 17 March 1972.

Damadian, R. 1973 Cation transport in bacteria. In *Critical reviews in microbiology* (March), pp. 377-422. C.R.C. Press.

Damadian, R., Goldsmith, M. & Zaner, K. S. 1971 Biological ion exchanger resins. II. Cell water and ion exchange selectivity *Biophys. J.* **11**, 739–760.

Damadian, R., Goldsmith, M. & Minkoff, L. 1977 NMR in cancer. XVI. FONAR image of the live human body. *Physiol. Chem. Phys.* **9**, 97–100.

Damadian, R., Minkoff, L., Goldsmith, M. & Koutcher, J. 1978 Field focusing nuclear magnetic resonance (FONAR) and the formation of chemical scans in man. *Naturwissenschaften* **65**, 250–252.

Damadian, R., Zaner, K., Hor, D. & DiMaio, T. 1974 Human tumors detected by nuclear magnetic resonance. *Proc. natn. Acad. Sci. U.S.A.* **71**, 1471–1473.

Goldsmith, M. & Damadian, R. 1975 NMR in cancer. VII. Sodium-23 magnetic resonance of normal and cancerous tissues. *Physiol. Chem. Phys.* **7**, 263–269.

Goldsmith, M., Koutcher, J. A. & Damadian, R. 1977 Nuclear magnetic resonance in cancer. XII: application of NMR malignancy index to human lung tumours. *Br. J. Cancer* **36**, 235–242.

Goldsmith, M., Koutcher, J. A. & Damadian, R. 1978*a* NMR in cancer. XIII: application of NMR malignance index to human mammary tumours. *Br. J. Cancer* **38**, 547–554.

Goldsmith, M., Koutcher, J. & Damadian, R. 1978*b* NMR in cancer. XI: application of the NMR malignancy index to human gastro-intestinal tumours. *Cancer* **41**, 183–191.

Hinshaw, W. S. 1974 Spin mapping: the application of moving gradients to NMR. *Phys. Lett.* A **48**. 84.

Hoult, D. I., Busby, S. J. W., Gadian, D. G., Radda, G. K., Richards, R. E. & Seeley, P. J. 1974 Observation of tissue metabolites using ^{31}P nuclear magnetic resonance. *Nature, Lond.* **252**, 285–287.

Koutcher, J. A. & Damadian, R. 1977 Spectral differences in the ^{31}P NMR of normal and malignant tissue. *Physiol. Chem. Phys.* **9**, 181–187.

Lauterbur, P. C. 1973 Image formation by induced local interactions: Examples employing nuclear magnetic resonance. *Nature, Lond.* **243**, 190–191.

Mallard, J., Hutchison, J. M. S., Edelstein, W. A., Foster, M. A., Ling, C. R. & Johnson, G. 1979 *Phil. Trans. R. Soc. Lond.* B **289**, 519–531.

Mansfield P. & Grannel, P. K. 1973 NMR 'diffraction' in solids? *J. Phys.* C **6**, L422.

Mansfield, P., Pykett, I. L. & Morris, P. G. 1978 Human whole body line-scan imaging by NMR. *Br. J. Radiol.* **51**, 921.

Zaner, K. S. & Damadian, R. 1975 Phosphorus-31 as a nucleur probe for malignant tumours. *Science, N.Y.* **189**, 729–731